

Regularization Through Simultaneous Learning: A Case Study on Plant Classification

Pedro Henrique Nascimento Castro^a, Gabriel Cássia Fortuna^b, Rafael Alves Bonfim de Queiroz^a, Gladston Juliano Prates Moreira^a, Eduardo José da Silva Luz^{a,*}

^a*Computing Department, Federal University of Ouro Preto (UFOP), Zip Code: 35400-000, Ouro Preto, MG, Brazil*

^b*Brazuca Lúpulos, Zip Code: 25610-080, Petrópolis, RJ, Brazil*

Abstract

In response to the prevalent challenge of overfitting in deep neural networks, this paper introduces Simultaneous Learning, a regularization approach drawing on principles of Transfer Learning and Multi-task Learning. We leverage auxiliary datasets with the target dataset, the UFOP-HVD, to facilitate simultaneous classification guided by a customized loss function featuring an inter-group penalty. This experimental configuration allows for a detailed examination of model performance across similar (PlantNet) and dissimilar (ImageNet) domains, thereby enriching the generalizability of Convolutional Neural Network models. Remarkably, our approach demonstrates superior performance over models without regularization and those applying dropout regularization exclusively, enhancing accuracy by 5 to 22 percentage points. Moreover, when combined with dropout, the proposed approach improves generalization, securing state-of-the-art results for the UFOP-HVD challenge. The method also showcases efficiency with significantly smaller sample sizes, suggesting its broad applicability across a spectrum of related tasks. In addition, an interpretability approach is deployed to evaluate feature quality by analyzing class feature cor-

*Corresponding author

Email addresses: pedro.hnc@aluno.ufop.edu.br (Pedro Henrique Nascimento Castro), g.fortuna@unesp.br (Gabriel Cássia Fortuna), rafael.queiroz@ufop.edu.br (Rafael Alves Bonfim de Queiroz), gladston@ufop.edu.br (Gladston Juliano Prates Moreira), eduluz@ufop.edu.br (Eduardo José da Silva Luz)

relations within the network’s convolutional layers. The findings of this study provide deeper insights into the efficacy of Simultaneous Learning, particularly concerning its interaction with the auxiliary and target datasets.

Keywords: Regularization, Overfitting, Multi-task Learning, Simultaneous Learning, Hop classification.

1. Introduction

Neural networks have achieved significant results in various computer vision problems [1, 2, 3, 4]. However, they often encounter a common issue: overfitting. Overfitting occurs when a model excels during training but performs substantially worse on test databases or real-world applications [5]. Several factors contribute to overfitting, including limited training data, model complexity, and data noise [6].

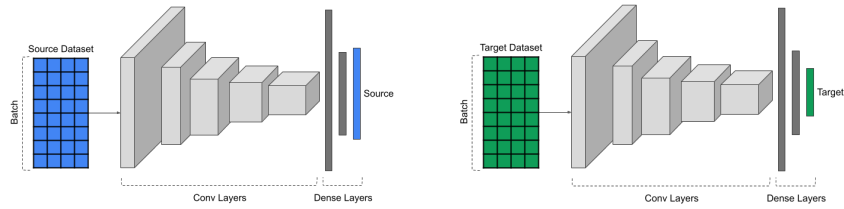
Regularization is among the most commonly used methods to reduce overfitting. Initially, the term referred to penalty terms added to the cost function of optimization problems. However, it now has a broader meaning and can encompass any modification made to a learning algorithm to reduce error on the test set rather than just during training [7]. Another definition posits that regularization is any technique that enables a model to generalize better [8].

Several regularization techniques exist, such as Weight Decay [9], Dropout [10, 11], Batch Normalization [12], Data Augmentation [13], Early Stopping [14], Adversarial Training [15], Transfer Learning [16], and Multi-task Learning [17]. Although these techniques have successfully reduced overfitting, none can completely or universally solve this problem. Each of these techniques may produce different results when applied to problems of diverse nature [18]. Therefore, combining two or more of these techniques is common to enhance a model’s performance [6]. Consequently, it is important to develop new techniques to achieve adequate generalization.

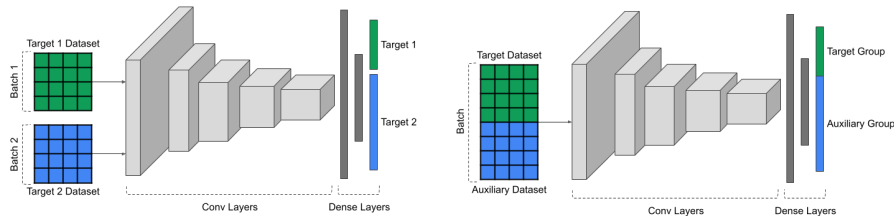
This study presents a regularization technique inspired by multi-task learning and transfer learning principles. Multi-task learning seeks to boost model

performance by capitalizing on the intrinsic structure of related tasks [19], as illustrated in Figure 1(b), paralleling how humans apply prior knowledge to learning. Transfer learning, depicted in Figure 1(a), entails training a model on a source dataset before fine-tuning it on a target dataset. Transfer learning speeds up the training process of deep learning models and improves the model’s ability to generalize [20]. Combining multi-task learning and transfer learning yields a robust approach to reducing overfitting. Although multi-task learning has successfully addressed overfitting within the same domain [21, 22, 23], training unrelated tasks concurrently may compromise performance, resulting in destructive interference or negative transfer [24, 25, 26, 27]. This issue is particularly pronounced when data originate from different domains, which is common in deep learning due to the widespread adoption of transfer learning and the accessibility of pre-trained ImageNet models [28, 29]. In light of the limitations and challenges highlighted in the paragraph above, an important research question arises: Is it possible to develop a composite loss function that effectively incorporates both target and auxiliary tasks, allowing for the simultaneous training of models using data from different domains? Investigating this question could lead to a more robust approach for addressing overfitting and improving model performance across various tasks and domains. In this study, we propose a method to address this issue within the context of a computer vision problem - the classification of hop varieties - by employing convolutional neural networks (CNNs) as depicted in Figure 1(c).

The approach entails modifying the model’s final layer, the classification layer, to accommodate more outputs, thus enabling the simultaneous classification of two labeled datasets: the target dataset (See Figure 1(c), in green) and the auxiliary dataset (See Figure 1(c), in blue). As a result, the classes in the last layer are divided into two groups: the target group (in green) and the auxiliary group (in blue). This configuration allows the model to train on both datasets simultaneously, with the only alteration being the input batch of the network. To achieve this, Simultaneous Learning Loss is designed, assigning different weights to each group and introducing a penalty for incorrect classifi-



(a) Transfer learning



(b) Multi-task learning

(c) Simultaneous Learning

Figure 1: (a) An example of the Transfer Learning technique, where the last trained layer from a source dataset is replaced by a target dataset for fine-tuning. (b) An instance of Multi-task Learning with two tasks, each with its respective input and output. (c) Simultaneous Learning technique, composed of a convolutional neural network with the last layer adapted to simultaneously classify images from the target group (in green) and the auxiliary group (in blue) during training.

cation between distinct groups. This approach aims to guide the model towards learning more general features from the target dataset rather than concentrating on specific aspects that may differentiate one class from another and potentially introduce noise. The objective is to optimize the model’s overall performance and reduce the likelihood of overfitting the training data. It is crucial to note that the final layer, though comprising two groups, represents a single task, as the classification of each group is not independent, unlike Multi-task Learning. Once the training process is complete, the component responsible for classifying the auxiliary dataset can be discarded.

Plant classification is a subject of interest within the field of machine learning, facilitating the detection of weeds among crops [30], the identification of vegetables with superior nutritional values [31], and enabling non-professionals

to easily discern between different species and varieties [32]. In line with this growing interest, for empirical validation, we use a dataset centered on classifying plant species, specifically hops—a crucial ingredient in beer brewing. With over 250 cataloged variants of hops [33] exhibiting significant leaf similarity among varieties [34], this classification task represents a substantial challenge. Therefore, it’s a relevant problem in the industry, demanding precision in identifying hop varieties. Beyond the application’s relevance, our chosen dataset (UFOP-HVD) offers an opportunity to assess our proposed methodology’s effectiveness across tasks within both similar and disparate domains. In particular, we draw upon PlantNet, which aligns with the UFOP-HVD’s domain, and ImageNet, representative of a distinct domain. Importantly, both ImageNet [28, 29] and PlantNet [35] possess parallel characteristics—a large number of images and classes—thus rendering the UFOP-HVD dataset an ideal selection for our research.

Regarding model interpretability and explicability, we explore a technique termed Layer Correlation, which facilitates understanding the relationships between the features learned by the model. This method assesses the correlation level of the features generated for each class, determining whether the model can produce pertinent information for prediction. Moreover, we demonstrate the classes from the auxiliary group that most significantly activate the primary group and present their corresponding activation maps.

In the context of hop variety classification, with the aid of the method proposed herein, we have enhanced the state-of-the-art results previously presented in [36]. The contributions of this work can be summarized as follows:

- A Simultaneous Learning method to regularize a model;
- A loss function that penalizes inter-group errors;
- A systematic approach to enhancing the interpretability of features learned at each model layer, promoting a deeper understanding of the learning process.

The structure of this paper is organized as follows: in Section 2, we review related works; in Section 3, we present the proposed cost function, Simultaneous Learning technique, evaluation metric, and Layer Correlation; in Section 4, we describe the datasets used, the experimental configurations and results, and the model interpretability; finally, in Section 5, we discuss the results obtained and propose possible future research directions.

2. Related Works

Multi-task Learning. The goal of Multi-task Learning is to perform the learning of two or more tasks simultaneously so that the learned weights can be shared among them. This aims to improve the model’s generalization on related tasks, sharing information during learning and allowing tasks to assist each other [17]. This approach is inspired by how humans use prior knowledge to learn new tasks [19]. However, the joint training of unrelated tasks may impair the model’s performance, generating an effect called destructive interference or negative transfer [24, 25, 26, 27].

Although some research explores unrelated tasks, as in [37, 38, 39], they employ a single input with distinct outputs. In this scenario, it is not feasible to use databases unrelated to the target database for training, as tasks, even though not related, are applied only to data from the same domain. The present study stands out from others by allowing the use of any auxiliary database, regardless of its relation to the target domain, facilitating the search for datasets, and expanding the possibilities of application in various areas. In addition, we consider classification as a single task, which allows the learned weights to be better utilized until the final layers since the tasks are not treated separately. To mitigate the problem of negative transfer, we propose an inter-group penalty, which encourages the model to differentiate the features of each group.

Next, we review some recent studies that apply multi-task learning in plant classification.

The study conducted by Zhu *et al.* [40] aims to classify plant species using

information about the plant family and a heatmap of the plant’s most important regions. First, a convolutional neural network with two outputs is trained, one for the family and one for the species, and a heatmap of the most activated regions is generated. Then, using the heatmap, a crop in the original plant image is generated and passed to a second CNN, which is also trained with family and species information. The datasets used were Malayakew, ICL, Flowers 102, and CFH plant.

The research by Lee *et al.* [41] combines plant species classification with disease identification. To do this, a CNN is used as the base model, specifically InceptionV3, which shares weights for both tasks. However, the result of the species classification is introduced before the disease classification layer in order to improve accuracy. A custom dataset with 5334 images distributed in 311 species and 289 diseases was constructed for the work.

In the work of [42], the authors also address the classification of plant species and disease identification. For this, they used the AlexNet architecture as the base model, which has two softmax outputs, one for each classification task. The cost function consists of a weighted sum of the corresponding cost functions for each task, both with a weight equal to 0.5. The datasets used were Plant Village and FISB, which contain samples of rice and maize.

The method proposed in [43] also involves plant classification and disease recognition, using the SE-ResNeXt-101 network with different outputs for each task. The cost function is a weighted sum of the two outputs, where the weighting takes values between 0 and 1. The datasets used were PlantVillage and PlantDoc.

Transfer Learning. Transfer Learning (TL) is a technique that aims to extract knowledge from a source task to a target task rather than performing concurrent learning, as in Multi-task Learning [16]. This technique usually involves training a model on a large labeled dataset (source task) and then fine-tuning it on a smaller, specific dataset (target task), transferring part of the acquired knowledge from one base to another. TL is often used to speed up the training and convergence of models with many parameters, using pre-trained

weights on the larger dataset. Our work falls into the category of Inductive Transfer Learning, where both target and auxiliary domain labels are available [44].

The study conducted by Kaya *et al.* [45] used a convolutional neural network architecture with three layers, as well as VGG-16 and AlexNet networks, to classify plant species in four different datasets: Flavia, Swedish Leaf, UCI Leaf, and Plantvillage. For this, two types of transfer learning were employed. In the first method, the models were pre-trained on the ImageNet dataset and subsequently fine-tuned on each of the plant datasets. In the second method, three of the plant datasets were used for pre-training and the remaining for fine-tuning.

In [46], the authors investigated the Plant Seedlings dataset, consisting of 12 crop species, and the Early Crop Weeds dataset, which includes 4 weed species. Four network architectures were tested: VGG19, Inception-ResNet, Xception, and Densenet. The networks were pre-trained on both ImageNet and an agricultural dataset for the transfer learning process. This agricultural dataset consists of one of the plant datasets (either crop or weed), which is used for pre-training, and the other plant dataset is used for fine-tuning.

The study by [47] presents a system for identifying crops and weeds that combines several convolutional neural networks, including Xception, Inception-Resnet, VGG16, VGG19, Mobilenet, and Densenet, with traditional machine learning classifiers such as Support Vector Machines, XGBoost, and Logistic Regression. All models were pre-trained with the ImageNet dataset. For this research, a custom dataset was created with images of tomato, cotton, and two weed species.

The work of [48] aims to detect and classify weeds in corn and soybean plantations. Detection was performed using YOLOv3, while the VGG16, ResNet50, and InceptionV3 networks were used for classification. All models were pre-trained with ImageNet. The dataset used in the research was created from images collected by the authors and images acquired through Google searches, totaling 462 images distributed among four weed species.

The approach proposed in [49] used the VGG-19 and InceptionV3 networks, pre-trained with ImageNet, to classify two varieties of Curcuma. The dataset used in the research was constructed from photographs taken with a smartphone in markets, totaling 647 images.

Finally, in the study by Chen *et al.* [50], methods were developed for weed identification in cotton plantations. Several models were evaluated, and the ResNeXt101 model, pre-trained with the ImageNet dataset, showed the best performance. A dataset with 5187 images of 15 weed species was created, and the images were collected under natural light conditions.

A common characteristic of the mentioned studies is the replacement of the final layers of the network to adapt it to the specific problem. During the fine-tuning process, some intermediate layers can be frozen, limiting the learning capacity of the model, or all layers can be retrained, resulting in partial forgetting of the knowledge acquired in the target domain. The present study distinguishes itself from the Transfer Learning approach by discarding the classification of the auxiliary dataset only after the completion of the full training and not before the fine-tuning. This methodology prevents the loss of knowledge acquired from the auxiliary dataset throughout the entire learning process.

Dropout. Dropout is one of the most used and successful regularization techniques in the deep learning area. We chose this technique to compare with our proposed method. During training, at each step, some neurons are randomly deactivated at each step so that the model learns representations with less overfitting capacity. This technique is a way to simulate a new, simpler model at each iteration. The standard version is used as a baseline for performance comparison. However, there are many variations, such as Dropconnect [51], Standout [52], Curriculum dropout [53], DropMaps [54], Autodropout [55] and LocalDrop [56].

The standard version of dropout has been applied in several plant classification problems, such as flower identification [57], medicinal plant classification [58], fruit recognition [59], differentiation between crops and weeds [60] and seedling identification [61]. Some studies suggest that combining different regu-

larization techniques can be efficient [62, 63, 64]. Therefore, dropout will also be tested in conjunction with our proposal to verify if the combination can result in better performance.

State of The Art For Hop variety Classification. The method proposed in [36] currently stands as the state-of-the-art solution for UFOP-HVD, facilitating a comprehensive, end-to-end process for hop variety classification. In this research, the authors conducted an exhaustive performance analysis of three eminent CNN architecture families: ResNets, EfficientNets, and InceptionNets. This investigation encompassed a series of ablation studies involving image classification, incorporating scenarios both with and without leaf segmentation, as well as with and without the application of data augmentation techniques. Additionally, the authors proposed an ensemble architecture combining six distinct CNN models, a methodology termed Multi-cropped-FULL. This model utilizes multiple leaves from the same image in conjunction with the entire image as input, resulting in an accuracy rate of 81%. Remarkably, with the integration of data augmentation techniques, the Multi-cropped-FULL model — considering all leaves of an image — reached an impressive accuracy of 95%. The authors also undertook a study termed “cropped configuration”, wherein each detected leaf of the image (potentially comprising multiple hop leaves) was transformed into a new input for the problem, enhancing the number of images. In the case of “cropped classification”, the employment of a ResNet50 architecture in conjunction with a 50% dropout rate culminated in the most efficacious results, garnering an accuracy rate of 78%.

3. Methodology

The simultaneous learning approach aims to train a model to learn representations of two groups to improve performance on one of them, referred to as the target group, while using the other group, the auxiliary group, to assist in this process. This paper proposes a regularization via simultaneous learning for deep learning models, specifically convolutional neural networks. In this con-

text, network architecture plays a crucial role. This section presents the loss functions and inter-group penalties. Then, the base and multi-group architectures are explored. The metrics used will be detailed, and Layer Correlation will be defined.

3.1. Simultaneous Learning Loss

Let f be a model that maps an input \mathbf{x} to a single output containing n classes, which can be divided into s groups (G_1, G_2, \dots, G_s). Denote the model weights by θ and the model’s output for the classes in group i as $[f(\mathbf{x}; \theta)]_{G_i}$. Let $\mathcal{L}_i([f(\mathbf{x}; \theta)]_{G_i})$ represent a loss function applied solely to the model’s outputs related to group i . The overall loss function, aiming to minimize the weighted sum of the loss functions for all groups, can be defined as:

$$\theta^* = \arg \min_{\theta} \left\{ \mathcal{F}(\theta, \bar{\lambda}) = \sum_{i=1}^s \lambda_i \mathcal{L}_i([f(\mathbf{x}; \theta)]_{G_i}) \right\}, \quad (1)$$

wherein $\bar{\lambda} = [\lambda_1, \lambda_2, \dots, \lambda_s]$ has the parameters assigned to each loss function i and θ^* denotes the model weights resulting from minimization.

In this work, we focus on two groups: a primary group, referred to as the target, and a secondary group, called the auxiliary. Consequently, the implementation of the loss function (Eq. 1) is expressed as:

$$\theta^* = \arg \min_{\theta} \left\{ \mathcal{F}(\theta, \bar{\lambda}) = \lambda_t \mathcal{L}_t([f(\mathbf{x}; \theta)]_{G_t}) + \lambda_a \mathcal{L}_a([f(\mathbf{x}; \theta)]_{G_a}) \right\}, \quad (2)$$

where $[f(\mathbf{x}; \theta)]_{G_t}$ and $[f(\mathbf{x}; \theta)]_{G_a}$ correspond to the outputs of the target and auxiliary groups, respectively, \mathcal{L}_t and \mathcal{L}_a are their respective loss functions, $\bar{\lambda} = [\lambda_t, \lambda_a]$. Let $\lambda \in [0, 1]$ a scalar be specified to the training of the model f . In this work, $\bar{\lambda}$ is given by $\bar{\lambda} = [\lambda, 1 - \lambda]$ to depend on only one hyperparameter to be adjusted.

In the simplest scenario, where only the target group is present, and no auxiliary group is considered, the loss function resembles a standard classification problem, with λ equal to 1. In this case, the categorical cross entropy [65, 66], depicted in Eq. (3), can be employed as the \mathcal{L}_t function. Categorical

Cross Entropy (CCE) quantifies the divergence between the probability distributions of the classes predicted by the model and the true labels of the training images. In the equation, k represents the number of target dataset classes, $\mathbf{y} = [y_1, y_2, \dots, y_k]$ is the ground-truth vector, $\hat{\mathbf{y}} = [\hat{y}_1, \hat{y}_2, \dots, \hat{y}_k]$ signifies the model’s predictions and t is the index of each class. The equation is defined as follows:

$$CCE(\mathbf{y}, \hat{\mathbf{y}}) = - \sum_{t=1}^k y_t \log(\hat{y}_t). \quad (3)$$

In this work, we propose a variant of the CCE loss function, termed Weighted Group Categorical Crossentropy (WGCC), designed explicitly for Simultaneous Learning. The corresponding equation is provided as follows:

$$WGCC(\mathbf{Y}, \hat{\mathbf{Y}}, \lambda) = -\lambda \sum_{t=1}^k y_t \log(\hat{y}_t) - (1 - \lambda) \sum_{a=k+1}^{k+m} y_a \log(\hat{y}_a), \quad (4)$$

where $\mathbf{Y} = [y_1, y_2, \dots, y_k, \dots, y_{k+m}]$, $\hat{\mathbf{Y}} = [\hat{y}_1, \hat{y}_2, \dots, \hat{y}_k, \dots, \hat{y}_{k+m}]$ and m is the number of classes in the auxiliary dataset.

In Eq. (4), the first term corresponds to the model output associated with the target dataset with k classes, while the second refers to the auxiliary dataset with m classes. Both terms are weighted by the hyperparameter λ , dictating the model’s preference for learning from one of the datasets during training.

In addition to the WGCC, we introduce an inter-group penalty term as per Eq. (5) to deter the model from erroneously classifying samples from the target group as belonging to the auxiliary group and vice versa. In this manner, even if the model misclassifies certain samples, it is urged to constrain its errors within each group. The penalty term is derived by calculating the cross-product between the sum of predictions for one group and the sum of the ground-truth vector for the other group. As a result, the product is maximized when all predictions are in one group, and the ground-truth value resides in the other. The hyperparameters α and β regulate the penalty factor. If the aim is to penalize only errors made on instances of the target group, simply set $\beta = 0$ and $\alpha > 0$. The same principle applies to errors committed on instances of the

auxiliary group, in this case, setting $\alpha = 0$ and $\beta > 0$. The equation of the Group Penalty (GP) factor is presented as follows:

$$GP(\mathbf{Y}, \hat{\mathbf{Y}}, \alpha, \beta) = \alpha \sum_{t=1}^k y_t \sum_{a=k+1}^{k+m} \hat{y}_a + \beta \sum_{t=1}^k \hat{y}_t \sum_{a=k+1}^{k+m} y_a. \quad (5)$$

The final loss function, referred to as the Simultaneous Learning Loss (SLL), is the sum of the WGCC and the GP, represented by the following equation:

$$\begin{aligned} SLL(\mathbf{Y}, \hat{\mathbf{Y}}, \mathbf{h}) = & -\lambda \sum_{t=1}^k y_t \log(\hat{y}_t) - (1 - \lambda) \sum_{a=k+1}^{k+m} y_a \log(\hat{y}_a) \\ & + \alpha \sum_{t=1}^k y_t \sum_{a=k+1}^{k+m} \hat{y}_a + \beta \sum_{t=1}^k \hat{y}_t \sum_{a=k+1}^{k+m} y_a, \end{aligned} \quad (6)$$

where $\mathbf{h} = [\alpha, \beta, \lambda]$ represent the hyperparameters vector of the model f .

3.2. Architecture

This study presents two architectures: the base model and the multi-group model. The former serves as a performance baseline, while the latter is employed in the Simultaneous Learning methodology in conjunction with the SSL given by Eq. (6).

The base model’s architecture comprises a series of convolutional layers responsible for extracting features from input images, which are resized to 300×300 pixels before processing. Following feature extraction, the output is channeled to a Global Average Pooling (GAP) layer [67] that reduces the dimensionality of the features and enhances the model’s robustness to variations in input image sizes. Subsequently, the GAP is connected to a sequence of two dense layers containing n_1 and n_2 neurons, respectively, utilizing the ReLU activation function. A final classification layer with k outputs is added, where k denotes the number of classes in the target dataset. The softmax activation function is applied to the classification layer outputs to determine each class’s probability. The loss function employed in this model is categorical cross-entropy. Figure 2(a) visually represents the base model.

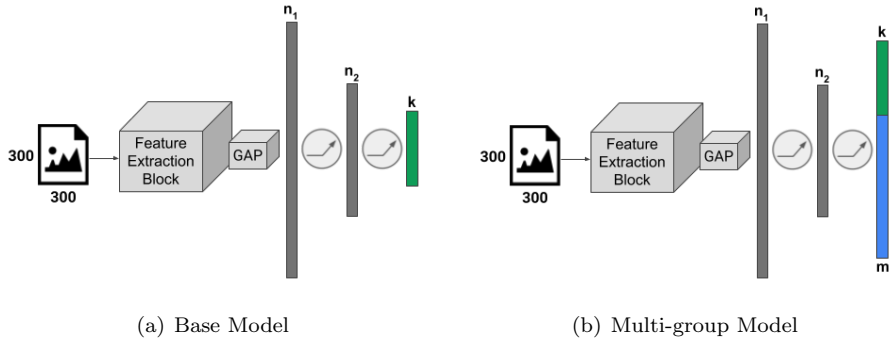


Figure 2: (a) Base model with a feature extraction block, a Global Average Pooling layer, and two dense layers, one with n_1 and another with n_2 neurons. The dense layers undergo a ReLU activation function. Ultimately, the model has a classification layer with k outputs. (b) Multi-group model, a modification of the base model where m outputs are added for the auxiliary group in the last layer, totaling $k + m$ outputs.

Figure 2(b) depicts the multi-group model. The primary distinction from the base model resides in the last layer, where m outputs are incorporated, with m representing the number of classes in the auxiliary dataset. As a result, the adapted model’s total number of outputs is $k + m$. Compared to the base network, the additional trainable parameters amount to $m \times (n_2 + 1)$, where n_2 denotes the number of neurons in the model’s penultimate layer. Notably, the number of parameters increase is linear concerning the classes of the auxiliary dataset, rendering the model’s size and training scalable. Upon completion of the training process, the m outputs and their corresponding parameters can be discarded, retaining only the outputs pertinent to the target dataset.

3.3. Training

The training procedure for both the base and multi-group models utilizes the gradient descent algorithm to update the neural network parameters. In contrast to the base model, which solely receives samples from the target dataset in each input batch, the multi-group model obtains a combination of samples from both the target and auxiliary datasets, maintaining a fixed proportion of 50% for each dataset. It is crucial to emphasize that this alteration in the batch

composition does not impact the model’s structure. The multi-group model processes all training images from the target dataset during each epoch. At the same time, at each step, the remaining half of the batch is supplemented with randomly selected images from the auxiliary dataset, ensuring no repetition per step.

The multi-group model’s computational strategy for the learning/training is systematized in Algorithm 1. In line 2 of this algorithm, the function *length* returns the size of the target dataset’s training set \mathbb{T} , i.e., the value T . In lines 6 and 8, it is used the notation $\mathbb{D}[I : J]$ to indicate that the images localized between the initial index I and final index J from the training set \mathbb{D} under analysis are collected. In line 7, the function *random* returns random images from the auxiliary dataset.

3.4. Metrics

In this study, we propose adapting the traditional accuracy metric, which we refer to as delimited accuracy (dacc). The dacc metric considers only some outputs (i.e., target group) from the neural network’s classification results. In contrast, outputs associated with the auxiliary dataset are deliberately excluded during inference. This approach ensures that only the outputs corresponding to the target dataset are considered for class determination throughout the validation phase. Delimited accuracy offers an additional advantage: it allows the model to be deployed in production without removing the auxiliary dataset outputs, thereby facilitating potential future retraining.

3.5. Interpretability

Layer Correlation. To achieve a deeper understanding of the features generated by the model’s convolutional layers, we put forth an approach that assesses the correlation of features produced for each class within each layer. Within this approach, each layer is represented by a vector comprising its outputs.

Algorithm 1 Pseudo-code for the multi-group model training

- 1: **Input:** Pre-trained model f with weights θ , target dataset's training set $\mathbb{T} = [(x_1^t, y_1^t), (x_2^t, y_2^t), \dots, (x_T^t, y_T^t)]$, auxiliary dataset's training set $\mathbb{A} = [(x_1^a, y_1^a), (x_2^a, y_2^a), \dots, (x_A^a, y_A^a)]$, hyperparameters vector $\mathbf{h} = [\alpha, \beta, \lambda]$, learning rate η , number of epochs N , batch size b
 - 2: $steps \leftarrow length(\mathbb{T})/b$ ▷ Number of steps per epoch definition
 - 3: $b \leftarrow b/2$ ▷ Batch size division by half
 - 4: **for** $epoch \leftarrow 1$ to N **do**
 - 5: **for** $s \leftarrow 1$ to $steps$ **do**
 - 6: $\mathbf{X}_s^t, \mathbf{Y}_s^t \leftarrow \mathbb{T}[(s-1)b : sb]$ ▷ Target group images/labels
 - 7: $\mathbb{A}^s \leftarrow random(\mathbb{A})$ ▷ Shuffling of samples in \mathbb{A}
 - 8: $\mathbf{X}_s^a, \mathbf{Y}_s^a \leftarrow \mathbb{A}^s[1 : b+1]$ ▷ Auxiliary group images/labels
 - 9: $\mathbf{X}_s, \mathbf{Y}_s \leftarrow \mathbf{X}_s^t + \mathbf{X}_s^a, \mathbf{Y}_s^t + \mathbf{Y}_s^a$ ▷ Images/labels concatenation
 - 10: $\hat{\mathbf{Y}}_s \leftarrow f(\mathbf{X}_s, \mathbf{Y}_s, \theta)$ ▷ Model f prediction
 - 11: $\mathcal{C} \leftarrow SLL(\mathbf{Y}_s, \hat{\mathbf{Y}}_s, \mathbf{h})$ ▷ Evaluation of the cost function using Eq. (6)
 - 12: $\mathbf{g} \leftarrow \nabla \mathcal{C}$ ▷ Gradients with respect to model f weights
 - 13: $\theta \leftarrow \theta - \eta \mathbf{g}$ ▷ Model f weights update
 - 14: **end for**
 - 15: **end for**
 - 16: **Output:** Trained model f with weights θ .
-

Initially, all images belonging to a single class from the test set of the target dataset are fed into the model for prediction. Subsequently, the positive outputs are summed for each channel within each layer. Ultimately, the summed value of the channel constitutes an element of a vector representing the layer. Figure 3 demonstrates this process for class C1, utilizing the third layer of a model containing five channels, each with a dimension of 3×3 . The negative elements of the channels are excluded, followed by summing all elements of each channel, which yields a vector where each channel is represented as an element.

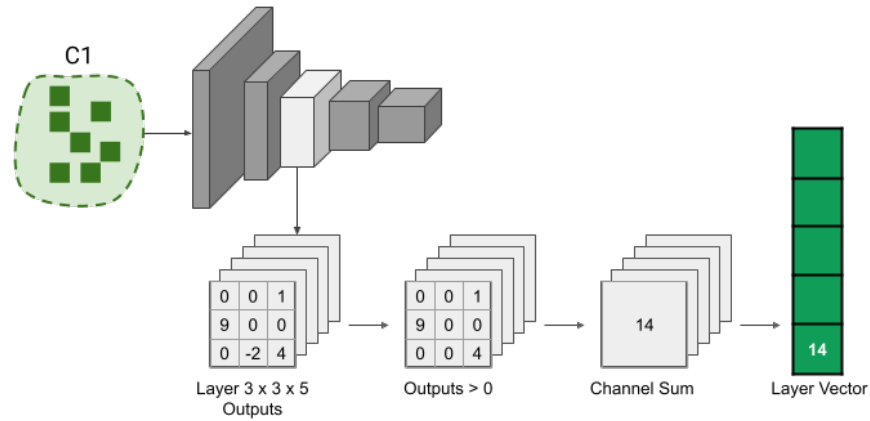


Figure 3: Example of transformation for class C1 of a layer with five channels of dimension 3×3 each into a five-element vector. Each channel has its positive values summed and becomes an element of the vector.

This procedure is repeated for every class, resulting in a list of vectors corresponding to each class, as demonstrated in the example in Figure 4 for classes C1, C2, and C3.

Subsequently, Pearson's correlation coefficients [68] are calculated between the vectors of each class. A scalar is derived from the mean of the absolute values of these coefficients. A higher value signifies a stronger correlation between the features generated by the layer under evaluation. High correlation may contribute to diminished model performance, as dependent variables or highly correlated ones offer little to no supplementary information about the classes

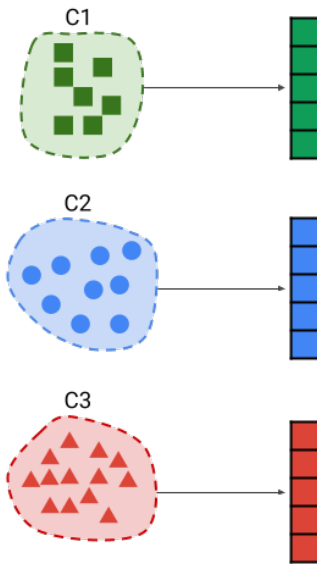


Figure 4: Example of vectors from a single layer of three different classes.

[69].

Grad-CAM. In this study, we also employ Grad-CAM (Gradient-weighted Class Activation Mapping) [70] to analyze the auxiliary dataset images that significantly activate the target group outputs. Grad-CAM utilizes the gradients of one or more selected outputs of the model, backpropagating them to the convolutional layers to generate a map of the most activated regions. This process enables the identification of the most significant portions of the image that prompted the model to produce specific outputs. Initially, images from the auxiliary dataset are fed into the model to generate predictions. Subsequently, only the outputs corresponding to the target group are filtered. The classes and images generating the highest values are selected for the Grad-CAM application, as they are most likely to confuse the model. Lastly, the images produced by Grad-CAM are included with a heatmap that identifies the activated areas.

4. Experiments and Results

This section describes the experimental design to address our research question. The implementation of the models and training procedures and the datasets employed in the experiments are also detailed. The performance of each model, in terms of accuracy and ROC/AUC curves, is presented and evaluated, considering variations of the hyperparameter λ . Finally, the results of the interpretability techniques, Layer Correlation, and Grad-CAM are showcased.

In this work, models were implemented using the TensorFlow library and trained on an NVIDIA GeForce GTX TITAN X graphics card with 12GB of memory. The experiments utilized the feature extraction blocks of the InceptionV3 [71] and ResNet50 [72] models, specifically their convolutional parts. The original dense layers were removed, and two new ones were added. The first dense layer employed 1024 neurons, while the second layer utilized 512 neurons directly connected to the classification layer. AdaGrad [73] was chosen as the optimizer, with a learning rate of 1×10^{-3} .

All models were pre-trained using the ImageNet dataset, and the weights of the dense layers were initialized with the Glorot Uniform technique [74]. The base model with InceptionV3 contained 24,397,484 trainable parameters, whereas ResNet50 had 26,163,724. The multi-group model increased by 513,000 parameters, totaling 24,910,484 for InceptionV3 and 26,676,724 for ResNet50. When applicable, dropout was applied to the dense layers. In all experiments, the batch size was set to 32 images. For the multi-group model, half of the batch was filled with images from the target dataset and the other half with the auxiliary dataset. The number of training epochs was established at 500, and the hyperparameters vector is fixed in $\mathbf{h} = [\alpha, \beta, \lambda] = [1, 1, \lambda]$. In Section 4.2, the influence of the hyperparameters λ is investigated on simulations.

4.1. Dataset

To assess the robustness of the proposed method in relation to the auxiliary task, two auxiliary datasets were selected: one related to the target dataset and

another unrelated. The UFOP Hop Varieties Dataset (UFOP-HVD) [75] was chosen as the target dataset, consisting of a database of hop leaves, a plant used in beer brewing. PlantNet-300K was selected for the related auxiliary dataset containing images of plants. In contrast, the unrelated auxiliary dataset employed was the well-known ImageNet, which includes various images, such as vehicles and animals, and is widely used in machine learning.

The UFOP-HVD dataset comprises 1592 images of young and mature hop leaves distributed across 12 unbalanced classes/varieties. The photographs exhibit no control over lighting, focus, distance, and angle, with resolutions ranging from 1040×520 to 4096×3072 . In this work, the original dataset split was utilized, allocating 70% of the images for training, 15% for validation, and 15% for testing. However, in some experiments, the training set was reduced to only 10% of its original size. Several samples from the dataset can be observed in Figure 5.

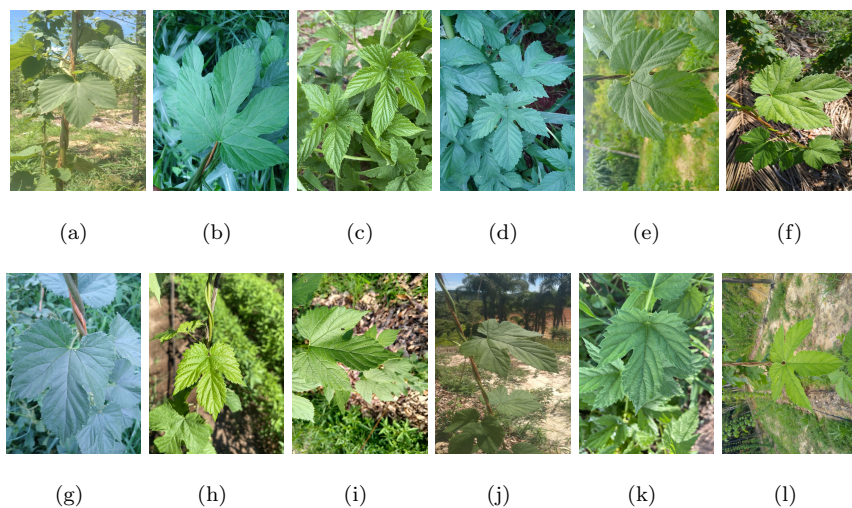


Figure 5: Examples of the 12 hop varieties used in this work: (a) Cascade; (b) Centennial; (c) Cluster; (d) Comet; (e) Hallertau Mittelfrueh; (f) Nugget; (g) Saaz; (h) Sorachi Ace; (i) Tahoma; (j) Triple Pearl; (k) Triumph; (l) Zeus.

Composed of 1,081 plant species and 306,146 images, the PlantNet-300K dataset is highly unbalanced, as some species have limited samples. The 1,000

classes with the fewest examples were selected, resulting in 72,680 images for the training set. A selection of samples from the dataset can be viewed in Figure 6.

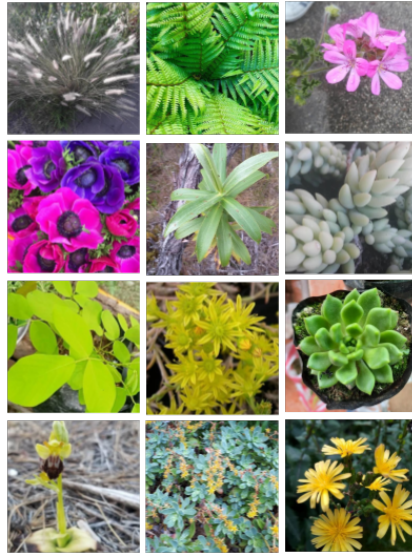


Figure 6: Examples of plant species from the PlantNet-300K dataset.

ImageNet, a dataset of over 14,197,122 images, is distributed across 1,000 classes and divided into training, validation, and testing sets. The dataset encompasses a diverse range of themes, including animals, vehicles, people, clothing, food, games, and technology equipment, among others. In this study, a subset containing 100 random samples from each class was utilized, amounting to 100,000 images. A selection of samples from the dataset can be viewed in Figure 7.

4.2. Sensitivity analysis of hyperparameter

The first experiment aimed to study the behavior of the hyperparameter λ for each model and auxiliary dataset. It varied from 0.1 to 1.0 in increments of 0.1. Figure 8 presents the accuracy plots of the models on the validation set as a function of λ variation. The red dashed line represents the result of the base model, where no regularization is applied, while the blue and green points refer

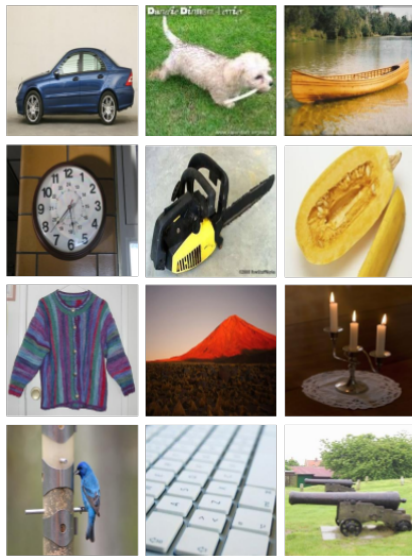
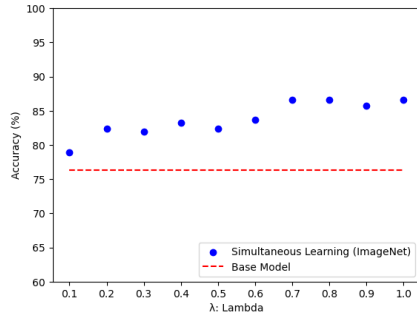


Figure 7: Examples of ImageNet images, from left to right and top to bottom: car, dog, boat, clock, chainsaw, pumpkin, sweater, volcano, candle, bird, keyboard, and cannon.

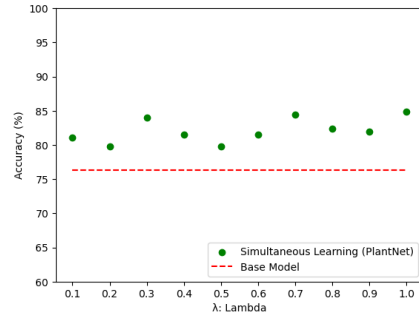
to the Simultaneous Learning technique using ImageNet and PlantNet-300K as auxiliary datasets, respectively. All combinations of the model, auxiliary dataset, and λ promoted some increase in accuracy. It is important to note that there was a significant performance gain for InceptionV3, which approached the performance of ResNet50, which does not occur in the base model. An improvement trend was also observed as λ increases. The best λ values found were 0.7 for ResNet50 with ImageNet, 1.0 for ResNet50 with PlantNet-300K, 0.7 for InceptionV3 with ImageNet, and 0.9 for InceptionV3 with PlantNet-300K. It is worth mentioning that when λ is equal to 1, the model ignores the classification of the auxiliary dataset, keeping only the penalty for inter-group errors. It seems that models with an auxiliary dataset more related to the target dataset benefit less from this classification.

4.3. Performance

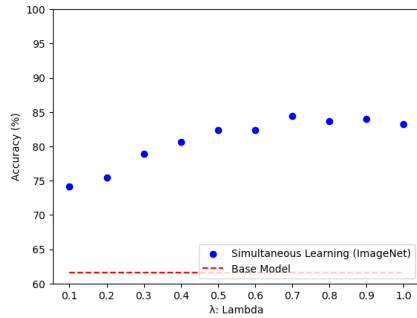
Subsequent experiments were performed on the test dataset, with the hyperparameter λ set to the optimal values identified in the previous investigation.



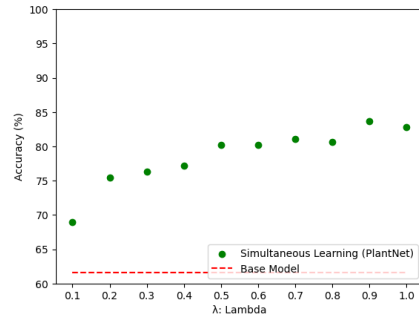
(a) Model: ResNet50



(b) Model: ResNet50



(c) Model: InceptionV3



(d) Model: InceptionV3

Figure 8: Delimited accuracy (vertical axis) on the validation set as a function of λ (horizontal axis). The dashed red line represents the result of the base model when no regularization is applied, and the blue and green points indicate the performance of the Simultaneous Learning technique using ImageNet and PlantNet as auxiliary bases, respectively.

Tables 1 and 2 display the accuracy of the ResNet50 and InceptionV3 models, respectively. The performance of the base models without regularization, which served as a baseline, is presented alongside the performance of the base models with dropout applied, using dropout rates of 0.2, 0.5, and 0.8, indicated in parentheses. The Simultaneous Learning technique’s performance, utilizing both auxiliary datasets, is significantly superior to the baseline and dropout, exhibiting at least a 5-percentage point difference in all comparisons and attaining up to 22 points higher than the baseline with InceptionV3.

The performance of the Simultaneous Learning method was evaluated on

Table 1: Comparison of ResNet50 model performance without regularization, with dropout, and with Simultaneous Learning technique.

Model	Accuracy (%)
Baseline	76.29
Dropout (0.2)	77.16
Dropout (0.5)	78.02
Dropout (0.8)	81.03
SL (PlantNet, $\lambda = 1.0$)	86.21
SL (ImageNet, $\lambda = 0.7$)	87.93

Table 2: Comparison of InceptionV3 model performance without regularization, with dropout, and with Simultaneous Learning technique.

Model	Accuracy (%)
Baseline	61.21
Dropout (0.2)	57.76
Dropout (0.5)	67.24
Dropout (0.8)	66.38
SL (PlantNet, $\lambda = 0.9$)	82.76
SL (ImageNet, $\lambda = 0.7$)	83.62

considerably smaller datasets by sub-sampling the training set to merely 10% of its original size, retraining the models, and applying the same regularizations. The results are in Tables 3 and 4. Simultaneous Learning once again exhibited superior performance. However, in certain instances, the application of dropout led to a decline in accuracy compared to the baseline.

4.4. Combined Performance

In the context of our study, examining the feasibility of combining multiple regularization techniques is of interest. To this end, the Simultaneous Learning method was integrated with dropout, and the results are displayed in Tables

Table 3: Comparison of ResNet50 model performance on a reduced dataset without regularization, with dropout, and with Simultaneous Learning technique.

Model	Accuracy (%)
Baseline	45.69
Dropout (0.2)	46.12
Dropout (0.5)	43.97
Dropout (0.8)	43.97
SL (PlantNet, $\lambda = 1.0$)	51.72
SL (ImageNet, $\lambda = 0.7$)	56.03

Table 4: Comparison of InceptionV3 model performance on a reduced dataset without regularization, with dropout, and with Simultaneous Learning technique.

Model	Accuracy (%)
Baseline	27.16
Dropout (0.2)	18.10
Dropout (0.5)	29.31
Dropout (0.8)	28.45
SL (PlantNet, $\lambda = 0.9$)	41.38
SL (ImageNet, $\lambda = 0.7$)	42.67

5 and 6. For the ResNet50, a superior outcome was achieved compared to the individual techniques when the dropout rate was set at 0.2 for both auxiliary datasets. For InceptionV3, the improvement in accuracy transpired only with the ImageNet dataset and a dropout rate of 0.8. The result remained unchanged with the PlantNet dataset and a dropout rate of 0.8.

4.5. ROC Curves / AUC

Given the unbalanced nature of the target dataset, evaluating the model’s performance in terms of sensitivity and specificity is crucial. To this end, ROC (Receiver Operating Characteristic) curves and AUC (Area under the ROC

Table 5: Comparison of ResNet50 model performance, combining Simultaneous Learning with dropout.

Model	Accuracy (%)
SL (PlantNet, $\lambda = 1.0$) + Dropout (0.2)	89.66
SL (PlantNet, $\lambda = 1.0$) + Dropout (0.5)	84.05
SL (PlantNet, $\lambda = 1.0$) + Dropout (0.8)	81.03
SL (ImageNet, $\lambda = 0.7$) + Dropout (0.2)	88.36
SL (ImageNet, $\lambda = 0.7$) + Dropout (0.5)	84.05
SL (ImageNet, $\lambda = 0.7$) + Dropout (0.8)	80.17

Table 6: Comparison of InceptionV3 model performance, combining Simultaneous Learning with dropout.

Model	Accuracy (%)
SL (PlantNet, $\lambda = 0.9$) + Dropout (0.2)	83.19
SL (PlantNet, $\lambda = 0.9$) + Dropout (0.5)	81.47
SL (PlantNet, $\lambda = 0.9$) + Dropout (0.8)	83.62
SL (ImageNet, $\lambda = 0.7$) + Dropout (0.2)	84.48
SL (ImageNet, $\lambda = 0.7$) + Dropout (0.5)	82.76
SL (ImageNet, $\lambda = 0.7$) + Dropout (0.8)	87.07

Curve) were constructed, as depicted in Figure 9, for both the ResNet50 and InceptionV3 models applied to the complete and reduced datasets. The red line represents the baseline, while the blue and green lines correspond to Simultaneous Learning with ImageNet and Simultaneous Learning with PlantNet, respectively. The results demonstrate that Simultaneous Learning displayed superior or, at the very least, equivalent performance to the baseline across the entire curve, with the AUC consistently higher in all cases.

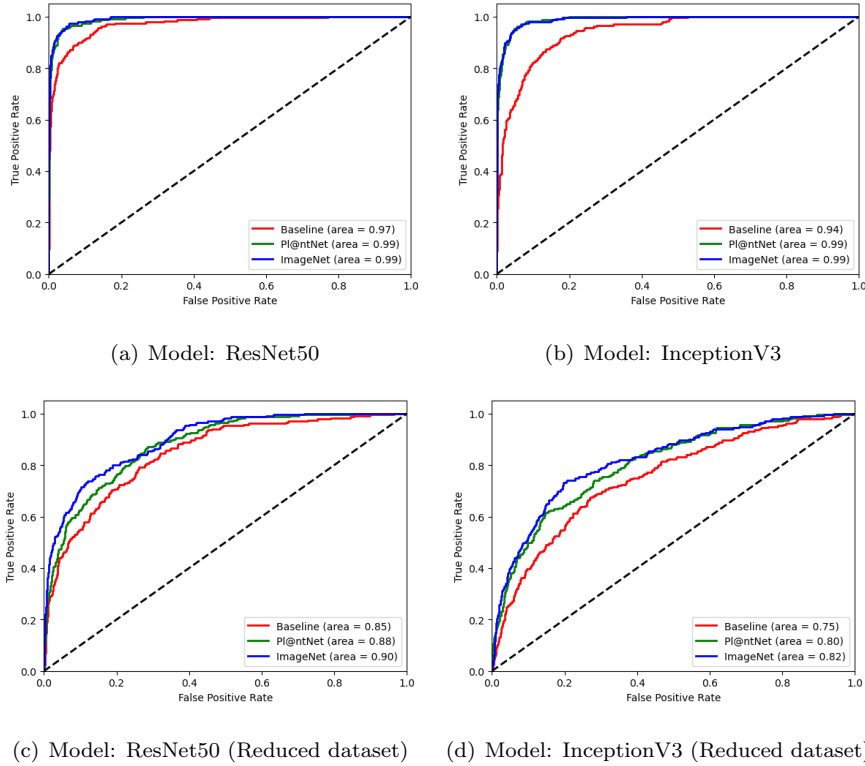


Figure 9: ROC curve and AUC of ResNet50 and InceptionV3 models. The red line corresponds to the baseline model. The green line applies Simultaneous Learning with the PlantNet dataset as the auxiliary base, and the blue line uses Simultaneous Learning with ImageNet.

4.6. Interpretability

In this study, the Layer Correlation technique is applied to both the base and multi-group models. The evaluation is conducted solely on the ResNet50 network, which contains 53 convolutional layers divided into five groups. For enhanced visualization, Figure 10(a) displays the correlation of the final layer in each group. A dramatic reduction in the correlation between classes in the last layer can be observed for the Simultaneous Learning method, with both ImageNet and PlantNet as auxiliary datasets. This finding justifies its superior performance, as less correlated features yield more pertinent information for class determination. Figure 10(b) provides a view of the network’s final 10

layers, revealing that Simultaneous Learning generated less correlated features in all of them.

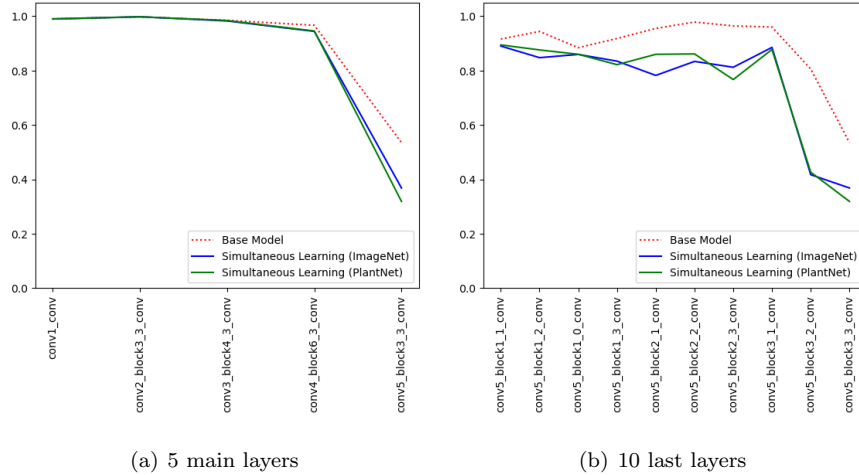


Figure 10: (a) Layer Correlation among class representations in the final layer of each of the five groups within the ResNet50 architecture. (b) Inter-class Layer Correlation within the last 10 layers of the ResNet50 model.

To investigate the relationship between the auxiliary dataset and the target dataset, the Grad-CAM technique is applied to the classes of the auxiliary dataset that most significantly activated the model’s outputs corresponding to the target group. Section Appendix A illustrates the top 10 classes from each auxiliary dataset with the highest activation. However, this section will focus solely on ImageNet, as PlantNet images predominantly consist of leaves and plants, which trivially relate to the target dataset. Figs. 11, 12, 13, 14, and 15 display selected images and their corresponding heatmaps, highlighting the regions that most contributed to the model’s interpretation of them as belonging to the target group. These classes are, respectively: coral fungus, custard apple, daisy, maitake mushroom, and sea anemone. A commonality among these classes is that they all represent organic elements. Although ImageNet encompasses numerous images of artificial objects, such as vehicles, equipment, and tools, the model did not associate them with the target dataset. It appears that

the model discerned a relationship between these living, organic materials, and hop leaves, despite the absence of shared color, shape, or texture attributes.

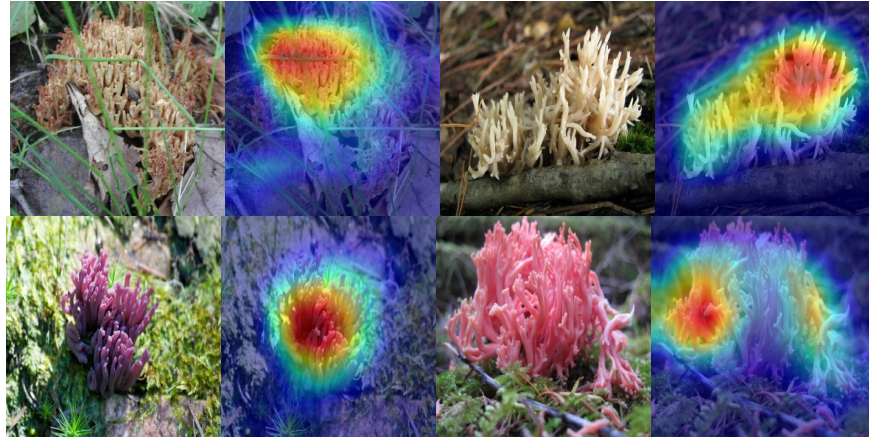


Figure 11: Examples of images from the Coral Fungus class drawn from the auxiliary dataset. Corresponding heatmaps are also displayed, which represent the regions that most strongly activated the outputs of the target group. These heatmaps were generated by employing the Grad-CAM method.



Figure 12: Examples of images from the Custard Apple class drawn from the auxiliary dataset. Corresponding heatmaps are also displayed, which represent the regions that most strongly activated the outputs of the target group. These heatmaps were generated by employing the Grad-CAM method.



Figure 13: Examples of images from the Daisy class drawn from the auxiliary dataset. Corresponding heatmaps are also displayed, which represent the regions that most strongly activated the outputs of the target group. These heatmaps were generated by employing the Grad-CAM method.



Figure 14: Examples of images from the Maitake class drawn from the auxiliary dataset. Corresponding heatmaps are also displayed, which represent the regions that most strongly activated the outputs of the target group. These heatmaps were generated by employing the Grad-CAM method.

5. Conclusion

In this study, we present the method of Simultaneous Learning, an innovative approach for enhancing the regularization of classification models by utilizing



Figure 15: Examples of images from the Sea Anemone class drawn from the auxiliary dataset. Corresponding heatmaps are also displayed, which represent the regions that most strongly activated the outputs of the target group. These heatmaps were generated by employing the Grad-CAM method.

existing datasets that may not be directly related to the target dataset. This method entails solely modifying the final layer of the model to accommodate the class groups and employing the Simultaneous Learning Loss for the training process. This approach results in a minimal increase in the number of parameters, thereby ensuring scalability. Additionally, it has a negligible impact on training, as the batch size remains constant. The proposed loss function incorporates an inter-group penalty designed to facilitate training by distinguishing between the target and auxiliary groups.

The findings were noteworthy, surpassing the performance of dropout—a commonly employed regularization technique—when applied to the UFOP-HVD, our target dataset. The method also demonstrated efficiency with significantly reduced sample sizes, offering promise for a range of similar challenges. Moreover, when tested in conjunction with dropout, the approach still yielded improvements in generalization, achieving state-of-the-art results for the UFOP-HVD dataset.

Furthermore, we introduced a novel technique called Layer Correlation to compare the quality of features generated by two models in a layer-by-layer

manner. This approach was employed to compare models with and without the Simultaneous Learning method, leading to significant findings. Of paramount importance is the versatility of Layer Correlation; it is not confined to the studied models and presents the potential for broader application across a variety of models featuring convolutional layers. Additionally, we tested the Grad-CAM method for visualizing how the auxiliary dataset triggers the outputs of the target group, providing a complementary perspective. Ultimately, both Layer Correlation and Grad-CAM were leveraged to provide greater interpretability to our results and process.

Within the scope of this research, we acknowledge certain limitations. Firstly, the hyperparameters λ related to the weight of each group and the inter-group penalties are manually adjusted, suggesting that further investigation into methods for automatically optimizing these values could be beneficial. Secondly, while the proposed model is well-suited for single-class classification problems, it may require reevaluation for multi-label issues where a single instance can contain more than one class. In addition, the method currently utilizes only one auxiliary database per training; future research could explore using multiple auxiliary databases to investigate their impact on performance.

In future research, the method of Simultaneous Learning could be evaluated across various datasets and contexts. Additionally, considering that only a subset of the auxiliary datasets was utilized, it would be intriguing to assess the method with more data and analyze the impact. Lastly, extending the model to encompass other types of networks, such as regression and object detection, could present an interesting path for investigation.

Declaration of Competing Interest

The authors declare that they have no known competing financial interests or personal relationships that could have appeared to influence the work reported in this paper.

Acknowledgments

The authors would also like to thank the *Coordenação de Aperfeiçoamento de Pessoal de Nível Superior* - Brazil (CAPES) - Finance Code 001, *Fundação de Amparo à Pesquisa do Estado de Minas Gerais* (FAPEMIG, grants APQ-01518-21), *Conselho Nacional de Desenvolvimento Científico e Tecnológico* (CNPq, grants 308400/2022-4) and Universidade Federal de Ouro Preto (PROPPI/UFOP) for supporting the development of this study.

References

- [1] Y. LeCun, Y. Bengio, G. Hinton, Deep learning, *nature* 521 (7553) (2015) 436–444.
- [2] R. Reedha, E. Dericquebourg, R. Canals, A. Hafiane, Transformer neural network for weed and crop classification of high resolution uav images, *Remote Sensing* 14 (3) (2022) 592.
- [3] N. Makanapura, C. Sujatha, P. R. Patil, P. Desai, Classification of plant seedlings using deep convolutional neural network architectures, in: *Journal of Physics: Conference Series*, Vol. 2161, IOP Publishing, 2022, p. 012006.
- [4] W. M. A. H. B. Wan, S. Nordin, et al., Plant recognition system using convolutional neural network, in: *IOP Conference Series: Earth and Environmental Science*, Vol. 1019, IOP Publishing, 2022, p. 012031.
- [5] P. Domingos, A few useful things to know about machine learning, *Communications of the ACM* 55 (10) (2012) 78–87.
- [6] Y. Tian, Y. Zhang, A comprehensive survey on regularization strategies in machine learning, *Information Fusion* 80 (2022) 146–166.
- [7] I. Goodfellow, Y. Bengio, A. Courville, *Deep Learning*, MIT Press, 2016, <http://www.deeplearningbook.org>.
- [8] J. Kukačka, V. Golkov, D. Cremers, Regularization for deep learning: A taxonomy, *arXiv preprint arXiv:1710.10686* (2017).
- [9] A. Krogh, J. Hertz, A simple weight decay can improve generalization, *Advances in Neural Information Processing Systems* 4 (1991).
- [10] N. Srivastava, G. Hinton, A. Krizhevsky, I. Sutskever, R. Salakhutdinov, Dropout: a simple way to prevent neural networks from overfitting, *The Journal of Machine Learning Research* 15 (1) (2014) 1929–1958.

- [11] D. Warde-Farley, I. J. Goodfellow, A. Courville, Y. Bengio, An empirical analysis of dropout in piecewise linear networks, arXiv preprint arXiv:1312.6197 (2013).
- [12] S. Ioffe, C. Szegedy, Batch normalization: Accelerating deep network training by reducing internal covariate shift, in: International Conference on Machine Learning, pmlr, 2015, pp. 448–456.
- [13] C. Shorten, T. M. Khoshgoftaar, A survey on image data augmentation for deep learning, Journal of Big Data 6 (1) (2019) 1–48.
- [14] T. Zhang, B. Yu, Boosting with early stopping: Convergence and consistency, The Annals of Statistics 33 (2005).
- [15] E. Wong, L. Rice, J. Z. Kolter, Fast is better than free: Revisiting adversarial training, in: International Conference on Learning Representations, 2020, pp. 1–17.
- [16] S. J. Pan, Q. Yang, A survey on transfer learning, IEEE Transactions on Knowledge and Data Engineering 22 (10) (2010) 1345–1359.
- [17] R. Caruana, Multitask learning, Springer, 1998.
- [18] R. Moradi, R. Berangi, B. Minaei, A survey of regularization strategies for deep models, Artificial Intelligence Review 53 (2020) 3947–3986.
- [19] S. Ruder, An overview of multi-task learning in deep neural networks, arXiv preprint arXiv:1706.05098 (2017).
- [20] T. Abbas, A. Fatima, T. Shahzad, K. Alissa, T. M. Ghazal, M. M. Al-Sakhnini, S. Abbas, M. A. Khan, A. Ahmed, et al., Secure iomt for disease prediction empowered with transfer learning in healthcare 5.0, the concept and case study, IEEE Access (2023).
- [21] H. Huang, H. Deng, J. Chen, L. Han, W. Wang, Automatic multi-task learning system for abnormal network traffic detection., International Journal of Emerging Technologies in Learning 13 (4) (2018).

- [22] X. E. Wang, V. Jain, E. Ie, W. Y. Wang, Z. Kozareva, S. Ravi, Environment-agnostic multitask learning for natural language grounded navigation, in: *Computer Vision–ECCV 2020: 16th European Conference, Glasgow, UK, August 23–28, 2020, Proceedings, Part XXIV 16*, Springer, 2020, pp. 413–430.
- [23] Y. Li, C. Caragea, A multi-task learning framework for multi-target stance detection, in: *Findings of the Association for Computational Linguistics: ACL-IJCNLP 2021*, 2021, pp. 2320–2326.
- [24] A. Kumar, H. Daume III, Learning task grouping and overlap in multi-task learning, *arXiv preprint arXiv:1206.6417* (2012).
- [25] X. Zhao, H. Li, X. Shen, X. Liang, Y. Wu, A modulation module for multi-task learning with applications in image retrieval, in: *Proceedings of the European Conference on Computer Vision (ECCV)*, 2018, pp. 401–416.
- [26] Y. Zhang, Q. Yang, An overview of multi-task learning, *National Science Review* 5 (1) (2018) 30–43.
- [27] Y. Zhang, Q. Yang, A survey on multi-task learning, *IEEE Transactions on Knowledge and Data Engineering* 34 (12) (2021) 5586–5609.
- [28] J. Deng, W. Dong, R. Socher, L.-J. Li, K. Li, L. Fei-Fei, Imagenet: A large-scale hierarchical image database, in: *2009 IEEE Conference on Computer Vision and Pattern Recognition, Ieee*, 2009, pp. 248–255.
- [29] O. Russakovsky, J. Deng, H. Su, J. Krause, S. Satheesh, S. Ma, Z. Huang, A. Karpathy, A. Khosla, M. Bernstein, et al., Imagenet large scale visual recognition challenge, *International Journal of Computer Vision* 115 (2015) 211–252.
- [30] X. P. Burgos-Artizzu, A. Ribeiro, A. Tellaeché, G. Pajares, C. Fernández-Quintanilla, Analysis of natural images processing for the extraction of agricultural elements, *Image and Vision Computing* 28 (1) (2010) 138–149.

- [31] K. Hameed, D. Chai, A. Rassau, A comprehensive review of fruit and vegetable classification techniques, *Image and Vision Computing* 80 (2018) 24–44.
- [32] H.-H. Lee, K.-S. Hong, Automatic recognition of flower species in the natural environment, *Image and Vision Computing* 61 (2017) 98–114.
- [33] J. Healey, *The Hops List: 265 Beer Hop Varieties From Around the World*, Julian Healey, 2016.
- [34] M. A. Jenks, *Plant nomenclature*, Purdue University-Department of Horticulture and Landscape Architecture. Disponível (2011).
- [35] C. Garcin, A. Joly, P. Bonnet, M. Servajean, J. Salmon, Pl@ntnet-300k image dataset (Apr. 2021). doi:10.5281/zenodo.4726653.
URL <https://doi.org/10.5281/zenodo.4726653>
- [36] P. H. N. CASTRO, G. J. P. Moreira, E. J. da Silva Luz, An end-to-end deep learning system for hop classification, *IEEE Latin America Transactions* 20 (3) (2021) 430–442.
- [37] B. R. Paredes, A. Argyriou, N. Berthouze, M. Pontil, Exploiting unrelated tasks in multi-task learning, in: *Artificial Intelligence and Statistics*, PMLR, 2012, pp. 951–959.
- [38] L. Liebel, M. Körner, Auxiliary tasks in multi-task learning, *arXiv preprint arXiv:1805.06334* (2018).
- [39] S. Chennupati, G. Sistu, S. Yogamani, S. Rawashdeh, Auxnet: Auxiliary tasks enhanced semantic segmentation for automated driving, *arXiv preprint arXiv:1901.05808* (2019).
- [40] Y. Zhu, W. Sun, X. Cao, C. Wang, D. Wu, Y. Yang, N. Ye, Ta-cnn: Two-way attention models in deep convolutional neural network for plant recognition, *Neurocomputing* 365 (2019) 191–200.

- [41] S. H. Lee, H. Goëau, P. Bonnet, A. Joly, Conditional multi-task learning for plant disease identification, in: 2020 25th international conference on pattern recognition (ICPR), IEEE, 2021, pp. 3320–3327.
- [42] A. S. Keceli, A. Kaya, C. Catal, B. Tekinerdogan, Deep learning-based multi-task prediction system for plant disease and species detection, *Ecological Informatics* 69 (2022) 101679.
- [43] D. Wang, J. Wang, Z. Ren, W. Li, Dhbp: A dual-stream hierarchical bilinear pooling model for plant disease multi-task classification, *Computers and Electronics in Agriculture* 195 (2022) 106788.
- [44] F. Zhuang, Z. Qi, K. Duan, D. Xi, Y. Zhu, H. Zhu, H. Xiong, Q. He, A comprehensive survey on transfer learning, *Proceedings of the IEEE* 109 (1) (2020) 43–76.
- [45] A. Kaya, A. S. Keceli, C. Catal, H. Y. Yalic, H. Temucin, B. Tekinerdogan, Analysis of transfer learning for deep neural network based plant classification models, *Computers and Electronics in Agriculture* 158 (2019) 20–29.
- [46] B. Espejo-Garcia, N. Mylonas, L. Athanasakos, S. Fountas, Improving weeds identification with a repository of agricultural pre-trained deep neural networks, *Computers and Electronics in Agriculture* 175 (2020) 105593.
- [47] B. Espejo-Garcia, N. Mylonas, L. Athanasakos, S. Fountas, I. Vasilakoglou, Towards weeds identification assistance through transfer learning, *Computers and Electronics in Agriculture* 171 (2020) 105306.
- [48] A. Ahmad, D. Saraswat, V. Aggarwal, A. Etienne, B. Hancock, Performance of deep learning models for classifying and detecting common weeds in corn and soybean production systems, *Computers and Electronics in Agriculture* 184 (2021) 106081.

- [49] A. Pratondo, E. Elfahmi, A. Novianty, Classification of curcuma longa and curcuma zanthorrhiza using transfer learning, *PeerJ Computer Science* 8 (2022) e1168.
- [50] D. Chen, Y. Lu, Z. Li, S. Young, Performance evaluation of deep transfer learning on multi-class identification of common weed species in cotton production systems, *Computers and Electronics in Agriculture* 198 (2022) 107091.
- [51] L. Wan, M. Zeiler, S. Zhang, Y. Le Cun, R. Fergus, Regularization of neural networks using dropout, in: *International Conference on Machine Learning*, PMLR, 2013, pp. 1058–1066.
- [52] J. Ba, B. Frey, Adaptive dropout for training deep neural networks, *Advances in Neural Information Processing Systems* 26 (2013).
- [53] P. Morerio, J. Cavazza, R. Volpi, R. Vidal, V. Murino, Curriculum dropout, in: *Proceedings of the IEEE International Conference on Computer Vision*, 2017, pp. 3544–3552.
- [54] R. Moradi, R. Berangi, B. Minaei, Sparsemaps: convolutional networks with sparse feature maps for tiny image classification, *Expert Systems with Applications* 119 (2019) 142–154.
- [55] H. Pham, Q. Le, Autodropout: Learning dropout patterns to regularize deep networks, in: *Proceedings of the AAAI Conference on Artificial Intelligence*, Vol. 35, 2021, pp. 9351–9359.
- [56] Z. Lu, C. Xu, B. Du, T. Ishida, L. Zhang, M. Sugiyama, Localdrop: A hybrid regularization for deep neural networks, *IEEE Transactions on Pattern Analysis and Machine Intelligence* 44 (7) (2021) 3590–3601.
- [57] Y. Liu, F. Tang, D. Zhou, Y. Meng, W. Dong, Flower classification via convolutional neural network, in: *2016 IEEE International Conference on Functional-Structural Plant Growth Modeling, Simulation, Visualization and Applications (FSPMA)*, IEEE, 2016, pp. 110–116.

- [58] R. Akter, M. I. Hosen, Cnn-based leaf image classification for bangladeshi medicinal plant recognition, in: 2020 Emerging Technology in Computing, Communication and Electronics (ETCCE), IEEE, 2020, pp. 1–6.
- [59] S.-H. Wang, Y. Chen, Fruit category classification via an eight-layer convolutional neural network with parametric rectified linear unit and dropout technique, *Multimedia Tools and Applications* 79 (2020) 15117–15133.
- [60] J. Haichen, C. Qingrui, L. Zheng Guang, Weeds and crops classification using deep convolutional neural network, in: Proceedings of the 3rd International Conference on Control and Computer Vision, 2020, pp. 40–44.
- [61] P. Chauhan, H. L. Mandoria, A. Negi, Deep residual neural network for plant seedling image classification, *Agricultural Informatics: Automation Using the IoT and Machine Learning (2021)* 131–146.
- [62] T. Van Laarhoven, L2 regularization versus batch and weight normalization, arXiv preprint arXiv:1706.05350 (2017).
- [63] T. He, Z. Zhang, H. Zhang, Z. Zhang, J. Xie, M. Li, Bag of tricks for image classification with convolutional neural networks, in: Proceedings of the IEEE/CVF Conference on Computer Vision and Pattern Recognition, 2019, pp. 558–567.
- [64] X. Li, S. Chen, X. Hu, J. Yang, Understanding the disharmony between dropout and batch normalization by variance shift, in: Proceedings of the IEEE/CVF Conference on Computer Vision and Pattern Recognition, 2019, pp. 2682–2690.
- [65] S. Bhatnagar, D. Ghosal, M. H. Kolekar, Classification of fashion article images using convolutional neural networks, in: 2017 Fourth International Conference on Image Information Processing (ICIIP), IEEE, 2017, pp. 1–6.
- [66] Y. Ho, S. Wookey, The real-world-weight cross-entropy loss function: Modeling the costs of mislabeling, *IEEE Access* 8 (2019) 4806–4813.

- [67] M. Lin, Q. Chen, S. Yan, Network in network, arXiv preprint arXiv:1312.4400 (2013).
- [68] J. L. Rodgers, W. A. Nicewander, Thirteen ways to look at the correlation coefficient, *American statistician* (1988) 59–66.
- [69] G. Chandrashekar, F. Sahin, A survey on feature selection methods, *Computers & Electrical Engineering* 40 (1) (2014) 16–28.
- [70] R. R. Selvaraju, M. Cogswell, A. Das, R. Vedantam, D. Parikh, D. Batra, Grad-cam: Visual explanations from deep networks via gradient-based localization, in: *Proceedings of the IEEE International Conference on Computer Vision*, 2017, pp. 618–626.
- [71] C. Szegedy, V. Vanhoucke, S. Ioffe, J. Shlens, Z. Wojna, Rethinking the inception architecture for computer vision, in: *Proceedings of the IEEE Conference on Computer Vision and Pattern Recognition*, 2016, pp. 2818–2826.
- [72] K. He, X. Zhang, S. Ren, J. Sun, Deep residual learning for image recognition, in: *Proceedings of the IEEE Conference on Computer Vision and Pattern Recognition*, 2016, pp. 770–778.
- [73] J. Duchi, E. Hazan, Y. Singer, Adaptive subgradient methods for online learning and stochastic optimization., *Journal of Machine Learning Research* 12 (7) (2011).
- [74] X. Glorot, Y. Bengio, Understanding the difficulty of training deep feed-forward neural networks, in: *Proceedings of the thirteenth international conference on artificial intelligence and statistics, JMLR Workshop and Conference Proceedings*, 2010, pp. 249–256.
- [75] P. Castro, E. Luz, G. Moreira, Dataset for hop varieties classification, *Data in Brief* 38 (2021) 107312.

Appendix A. Auxiliary classes with the highest activation of the target group.



Figure A.16: Top 10 ImageNet classes that activated the target group the most. Each row corresponds to a class and its 10 instances with the highest activation.



Figure A.17: Top 10 PlantNet classes that activated the target group the most. Each row corresponds to a class and its 10 instances with the highest activation.